sustainability

MDPI

Article

3D-Printed Programmable Mechanical Metamaterials for Vibration Isolation and Buckling Control

Ali Zolfagharian [1,*], Mahdi Bodaghi [2,*], Ramin Hamzehei [2,3], Liam Parr [1], Mohammad Fard [4] and Bernard F. Rolfe [1,*]

[1] School of Engineering, Deakin University, Geelong, VIC 3216, Australia; lparr@deakin.edu.au
[2] Department of Engineering, School of Science and Technology, Nottingham Trent University, Nottingham NG11 8NS, UK; hamzeher@myumanitoba.ca
[3] Department of Mechanical Engineering, University of Manitoba, Winnipeg, MB R3T 5V6, Canada
[4] School of Engineering, Royal Melbourne Institute of Technology, Melbourne, VIC 3000, Australia; mohammad.fard@rmit.edu.au
* Correspondence: a.zolfagharian@deakin.edu.au (A.Z.); mahdi.bodaghi@ntu.ac.uk (M.B.); bernard.rolfe@deakin.edu.au (B.F.R.)

Abstract: Vibration isolation performance at low-frequency ranges before resonance is a vital characteristic that conventional springs cannot exhibit. This paper introduces a novel zero Poisson's ratio graded cylindrical metamaterial to fulfill two main goals: (1) vibration isolation performance in low-frequency bands prior to resonance and (2) global buckling control of a long cylindrical tube. For this purpose, "soft and stiff" re-entrant unit cells with varying stiffness were developed. The cylindrical metamaterials were then fabricated using a multi-jet fusion HP three-dimensional (3D) printer. The finite element analyses (FEA) and experimental results demonstrate that the simultaneous existence of multi-stiffness unit cells leads to quasi-zero stiffness (QZS) regions in the force-displacement relationship of a cylindrical metamaterial under compression. They possess significant vibration isolation performance at frequency ranges between 10 and 30 Hz. The proposed multi-stiffness re-entrant unit cells also offer global buckling control of long cylindrical tubes (with a length to diameter ratio of 3.7). The simultaneous existence of multi-stiffness re-entrant unit cells provides a feature for designers to adjust and control the deformation patterns and unit cells' densification throughout cylindrical tubes.

Keywords: vibration isolation; low frequencies; metamaterials; multi-stiffness unit cells; global buckling; 3D printing

Citation: Zolfagharian, A.; Bodaghi, M.; Hamzehei, R.; Parr, L.; Fard, M.; Rolfe, B.F. 3D-Printed Programmable Mechanical Metamaterials for Vibration Isolation and Buckling Control. *Sustainability* **2022**, *14*, 6831. https://doi.org/10.3390/su14116831

Academic Editor: Pablo Rodríguez-Gonzálvez

Received: 13 May 2022
Accepted: 31 May 2022
Published: 2 June 2022

1. Introduction

For decades, the modification and development of new materials with intrinsic properties have been predominately carried out by altering the chemical composition of the material. This practice has enabled the development of a large market for materials that can be applied to diverse and complex applications [1]. On the contrary, mechanical metamaterials propose a unique alternative to "traditional" materials and offer distinctive properties [2]. Mechanical metamaterials are artificially engineered structures developed by repeating units of mechanical sub-structures [2]. Unlike conventional materials, the macroscopic properties of metamaterials are predominately based on the specific design of the cells, not their chemical composition.

Mechanical properties can be programmed to a wide variety of conventional designs via the use of 3D printing technology. Mechanical metamaterials are divided into several main groups, including positive Poisson's ratio (PPR) structures such as honeycombs [3–6], zero Poisson's ratio (ZPR) structures [7–9], and negative Poisson's ratio (NPR) structures, so-called auxetics [10–13]. Metamaterials have been used for various applications, including

electromagnetic fields for achieving negative permeability, acoustics, and vibration isolation [14–16]. Vibration isolation in low-frequency ranges can be controlled by designing mechanical metamaterials in specific ways based on several constraints and considerations such as negative or quasi-zero stiffness (QZS) metamaterials [17–22].

Off-road vehicles' suspensions are designed to be very hard and inflexible to resist the rough road conditions they operate in, reducing the chassis suspension's capacity to efficiently isolate vibrations. Meanwhile, the vibration magnitude in such vehicles is multiple times more severe than in ordinary passenger vehicles driving on good motorable roads. Therefore, drivers operating in sectors such as mining, construction, and agriculture who spend many hours a day on the road are particularly vulnerable to the potentially harmful vibrations that result from poor road conditions. Studies have shown low frequency, whole-body vibrations could cause various health issues, including increased tiredness, fatigue, motion sickness, vertebrae diseases, digestive and vision issues, balance impairment, and a reduction in reaction times [23]. Due to the glaring consequences of vibration on the health of off-road vehicle drivers, industry players have considered it a critical factor in the design and manufacturing of automotive vehicles. Vehicle occupants often experience vibrations in the frequency range of 0 to 20 Hz which mainly affect health due to the resonant frequency of human organs. This indicates the importance of proper vibration isolators in vehicles to attenuate vibrations within this low-frequency band [23].

From a mechanical point of view, traditional linear spring vibration isolation systems are incapable of significantly suppressing low-frequency vibrations. To overcome this limitation of traditional isolators with low-cost passive systems, nonlinear isolators can be used [21]. QZS isolators with characteristics of high-static and low-dynamic stiffness have nearly zero overall dynamic stiffness without affecting the loading capacity of the system due to their inherent high-static stiffness. The high-static and low-dynamic combination of these non-linear systems promises low-frequency vibration isolation [21]. Typical QZS mechanisms combine a positive and negative stiffness element to produce a net zero stiffness [24].

A quasi-zero stiffness isolator is identified by the zero stiffness "plateau" region on a force-displacement curve following a static compression test. When a mass is placed on the QZS isolator, it causes the system to compress and situate in the plateau region; the dynamic stiffness of the isolator then becomes zero or near zero. The force resulting in the plateau region is often referred to as the "QZS payload" [21]. Quasi-zero stiffness mechanisms can be devised through a variety of different mechanisms and designs. The vast majority of QZS isolators are currently being developed by combining oblique and vertical springs, the buckling of beams, or via magnet rings [25]. QZS can also be achieved through the design of mechanical metamaterials, enhanced by developments in 3D printing technologies allowing for the manufacturing of complex cellular geometries. Unlike the spring system, negative stiffness can also be realized in metamaterials by buckling the unit cell [24,26]. For a mass to be isolated from vibrations using a metamaterial structure with QZS, its mass must be primarily supported by the positive stiffness element.

The main contribution of this work is the control of low-frequency vibration isolation in cylindrical metamaterials harnessed through the control of global buckling. This study aims to introduce new QZS graded cylindrical metamaterials with ZPR for potential applications as passive vibration attenuators in vehicles within the low-frequency band, the comfort zone of the human body, ranging from 10 to 30 Hz. To do so, the simultaneous presence of multi-stiffness unit cells, "soft and stiff re-entrant unit cells", is devised, leading to the appearance of a QZS, plateau, region in the force-displacement relationship. The multi-stiffness unit cells provide adjustable deformation patterns and global buckling control throughout the cylindrical metamaterials by considering a specific arrangement of soft and stiff unit cells, resulting in isolating external excitations at low-frequency ranges. The designed cylinders will be fabricated using 3D printing, and the FEA and experimental results will be conducted to demonstrate the contributions.

The rest of the paper is organized as follows: Section 2 describes the materials used, fabrication details, and the geometries of the cylinders, as well as the finite element simulation results. Section 3 presents the results of the experiments and discusses them with the FEA results of different cylinder designs. The main achievements of the study are summarized in Section 4.

2. Materials and Methods

2.1. Unit Cell Designs

From a structural standpoint, architected structures gain their mechanical properties from the specific unit cells' geometry rather than the parent material used for fabrication. Gradients are considered in the design of the cylinders by introducing diversity in unit cells' designs, cell wall thicknesses, or both. This could be employed to enhance such mechanical properties as energy absorption performance and crashworthiness behavior. The graded cylindrical metamaterials are developed in this study by introducing two multi-stiffness re-entrant unit cells, so-called "soft and stiff unit cells", as shown in Figure 1. The unit cell parameters are also provided in Table 1.

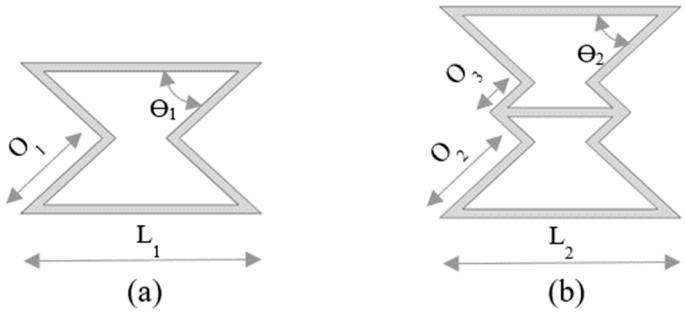

Figure 1. (**a**) Soft and (**b**) stiff re-entrant unit cells.

Table 1. "Soft and stiff unit cells" parameters.

Symbols	L_1	L_2	O_1	O_2	O_3	Θ_1	Θ_2
Values (mm)	22	22	11.3	11.3	4.5	45	45

2.2. Design of the Graded Cylindrical Metamaterials

According to the re-entrant unit cells, some different designs for graded ZPR cylinders [12,13] are proposed for the consideration of QZS properties as depicted in Figure 2. Since ZPR cylinders were investigated earlier, the QZS characteristic of the ZPR cylinders is the main contribution of this study, achieved via buckling control and "soft and stiff unit cells". To have comparable results, it is worth mentioning that the mass of all cylinders was kept constant by either increasing or decreasing the wall thickness. In this regard, the mass of all cylinders is the same, 50 g, except for long cylinders with a 100 g mass.

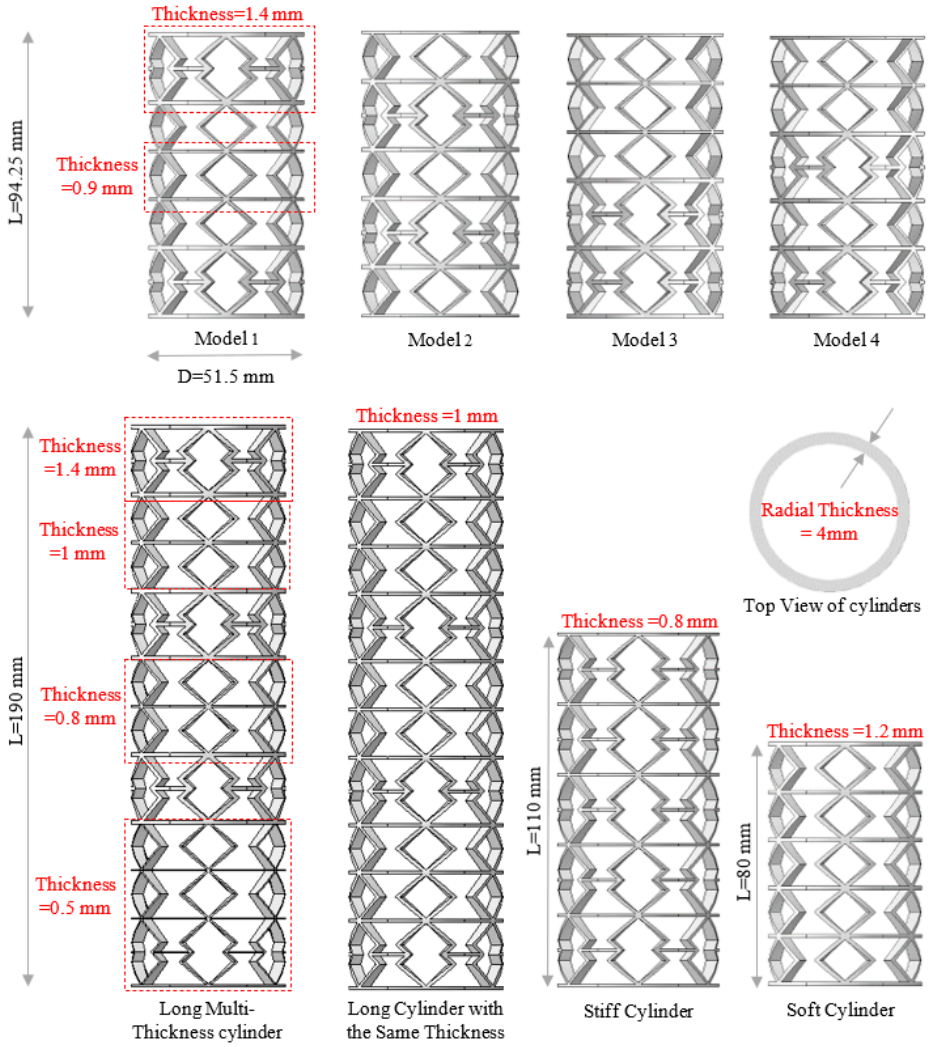

Figure 2. Various designs and models of graded cylindrical metamaterials.

2.3. Fabrication Process

A multi-jet fusion (MJF) 3D printer was used to fabricate the cylindrical metamaterials from Polyamide 12 (PA12). Table 2 provides information on the MJF 3D printing parameters used in this study.

Table 2. MJF 3D printer set-up parameters.

Properties	Value/Type
Fresh Material	20%
Print Profile	Mono Balanced
Cooling Profile	Natural Cooling
Packing Density	10.42%

2.4. Material Behaviors

Polyamide 12 (PA12) was the parent material. To obtain the mechanical properties of PA12, five material tensile-testing samples were designed as per ASTM D638-14. The samples were prepared with the dimensions provided in Figure 3a and 3D-printed as shown in Figure 3b. A test speed of 5 mm/min was applied during the tensile tests and the force-displacement behavior of the cylinders was measured using the Instron 5567 50 kN load frame. The stress-strain relationship of the PA12 is provided in Figure 3c. As can

be seen, the material exhibited linear behavior in the beginning, followed by a softening non-linear response until the break-down point quite similarly in all the samples.

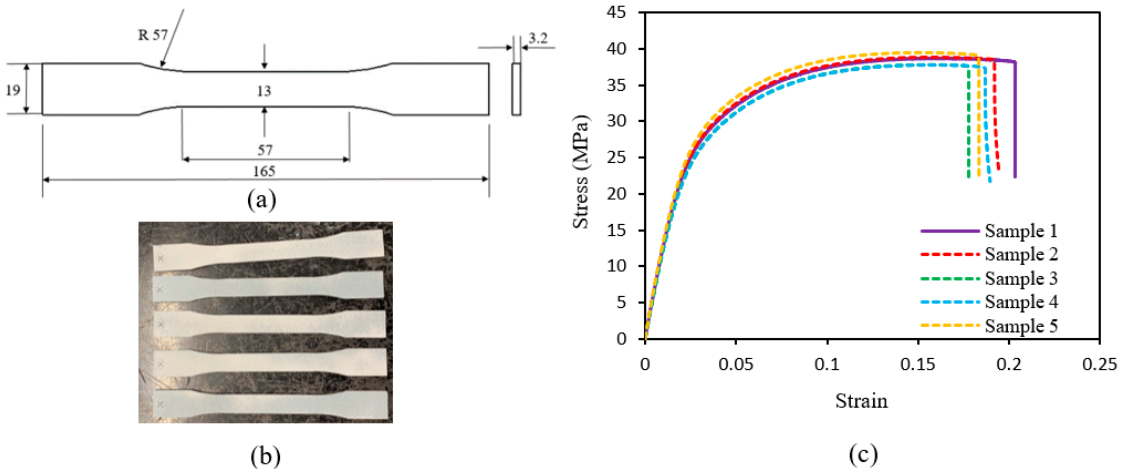

Figure 3. (**a**) Schematic view of ASTM d638-14, (**b**) 3D-printed tensile tests, and (**c**) PA12 stress-strain relationship.

2.5. Cylindrical Metamaterials, Mechanical and Vibration Tests

PA12-based cylindrical metamaterials fabricated by the MJF 3D printer are shown in Figure 4. The geometrical specifications are the same as shown in Figure 2.

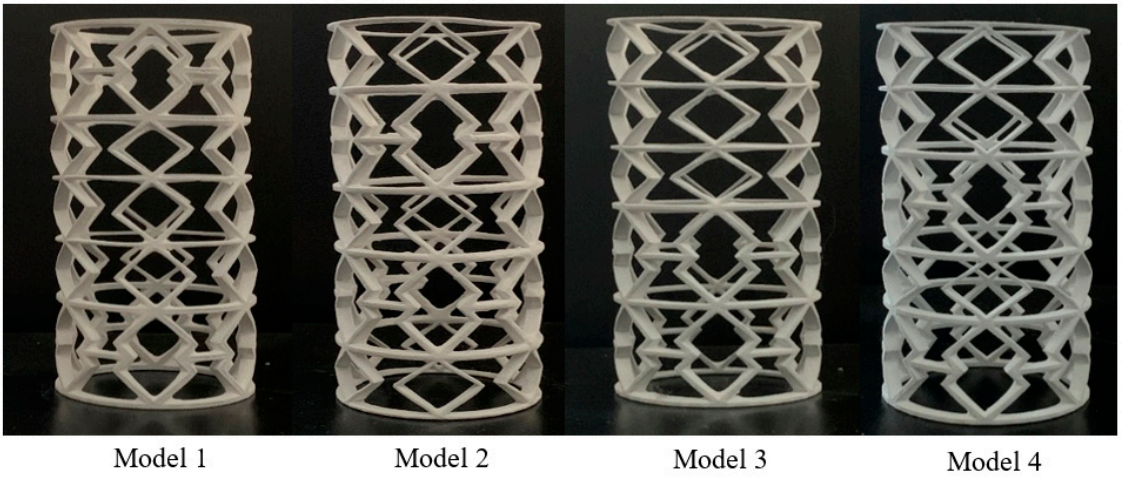

Figure 4. 3D-printed cylindrical metamaterials.

After printing the cylindrical metamaterials, quasi-static compression tests were conducted on the 3D-printed cylinders using the Instron 5567 50 kN load frame, with a displacement rate of 5 mm/min as well (see Figure 5).

To conduct the vibration analysis, a vibration shaker (S 5220-120 Vibration Exciter, TIRA GmbH, Schalkau, Germany) was used, coupled with an amplifier (BAA 1000-E Amplifier, TIRA GmbH, Schalkau, Germany) and controller (Vibration Research 9500, Jenison, MI, USA), to precisely control and record the vibration accelerations applied to the cylindrical metamaterials. The experimental setup is shown in Figure 6. The metamaterials are placed on top of the shaker using supports cut out from lightweight medium-density fiberboard to increase the surface area on which the input vibrations were applied. Four cylindrical metamaterials were placed on top of the shaker for each model analysis to achieve stability during vibration tests. Accelerometers were then attached to the top and bottom of the supporting plates to record the input (bottom plate connected to the shaker)

and output (top plate above the metamaterial) accelerations. The data were then recorded and compiled to understand the vibration level difference (VLD) between the plates.

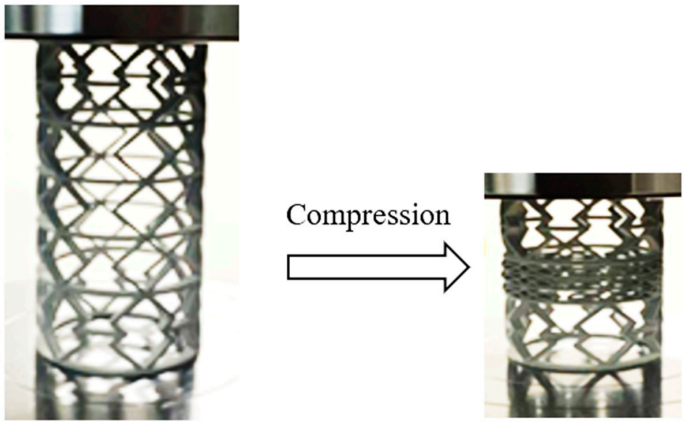

Figure 5. Quasi-static compression tests on cylindrical metamaterials.

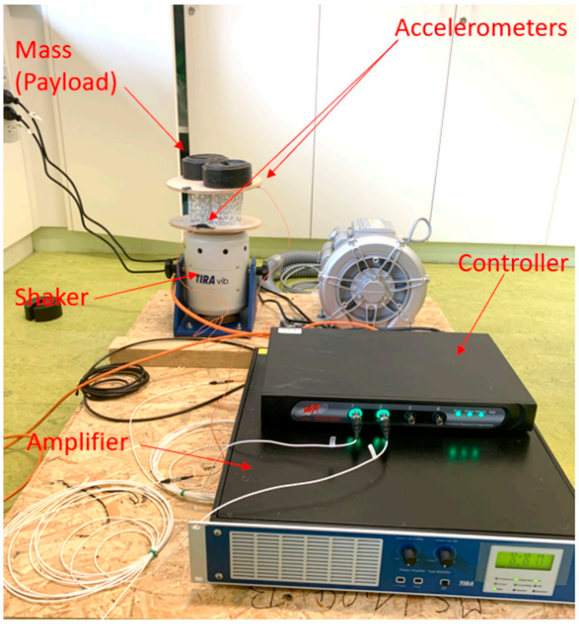

Figure 6. Mechanical vibration experimental set-up.

Using the Tira vibration shaker set-up as shown in Figure 6, the vibration level difference (VLD) was determined by recording the acceleration applied to the bottom plate directly via the shaker (input acceleration) and the acceleration sensed on the top plate above the cylindrical metamaterials (output acceleration). The vibration level difference could then be calculated from Equation (1).

$$\mathrm{VLD} = 20 \log \left(\frac{a_{output}}{a_{input}} \right) \quad (1)$$

For frequency ranges in which the VLD was below zero, vibration isolation was achieved ($a_{output}/a_{input} < 1$). This means that the vibrational accelerations experienced on the top plate above the metamaterials were less than the input accelerations on the bottom plate applied by the Tira shaker. Figure 7 exhibits the incapability of the springs to isolate external excitations at low-frequency ranges.

As this project primarily aimed to achieve vibration isolation at low frequencies, particularly those ranging from 0 to 20 Hz, vibration tests were conducted by applying constant accelerations to the base plate. The accelerations were applied using a sine sweep between 0 and 30 Hz. Results were determined for four input accelerations related to the varying subjective comfort levels of the human body, including fairly comfortable, less comfortable, not comfortable, and uncomfortable, as provided in Table 3.

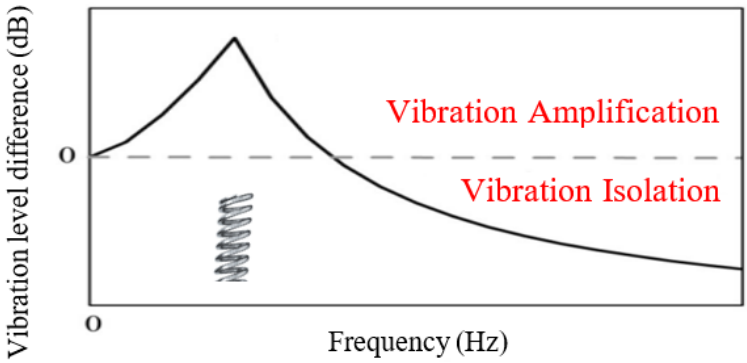

Figure 7. VLD-frequency relationship of springs.

Table 3. Comparison of the weighted acceleration experienced by the human body [27].

Weighted Acceleration Value	The Subjective Experience of the Human Body
<0.315	Very Comfortable
0.315–0.63	Fairly Comfortable
0.5–1	Less Comfortable
0.8–1.6	Not Comfortable
1.25–2.5	Uncomfortable
>2	Very Uncomfortable

2.6. Finite Element Analysis

Compression processes of cylindrical tubes were simulated using ABAQUS/Explicit software version 6.12 (Dassault Systemes, Vélizy-Villacoublay, France) [28]. For this purpose, two rigid plates were considered. Then, two reference points were assigned to the rigid plates to apply boundary conditions and compressive displacements. The cylindrical tubes were then confined between two rigid plates. The bottom reference point was fully constrained along with the three principal directions, whereas the top one moved downwards to compress the cylindrical tubes as illustrated in Figure 8. A general contact was established between the rigid plates, cylindrical metamaterials, and the cell walls to prevent interpenetration.Furthermore, as PA12 is the parent material, a proper value of the friction coefficient, 0.15, was considered [29].

As the cell walls in cylindrical tubes possess pure bending under compression, three-dimensional (3D) solid continuum hexahedral elements containing eight nodes with second-order accuracy, exhibiting accurate results in bending, so-called the C3D8R, are considered. For rigid plates, the R3D4 element type was selected. In an FEA, the response surface of a model will be divided into several fine regions to obtain the most accurate results during analysis. This surface division of a model is called the "element seed size". To achieve accurate results, a convergence study was conducted to find the best and most efficient element size. The seed sizes were changed from 1 mm to 0.4 mm, with an interval of 0.3 mm. Due to the great coincidence between the FEA and the experiment when the 0.4 mm seed size was considered, see Figure 9, this seed size was selected for carrying out the FEA on the cylindrical metamaterials.

As a dynamic explicit module was used to perform the FEAs, the velocity must be correlated to an actual quasi-static compression test condition. Figure 10 compares the kinetic and internal energies of "model 1" cylindrical metamaterials under quasi-static compression at a velocity of 1000 mm/s, where kinetic energy is negligible compared to the internal energy.

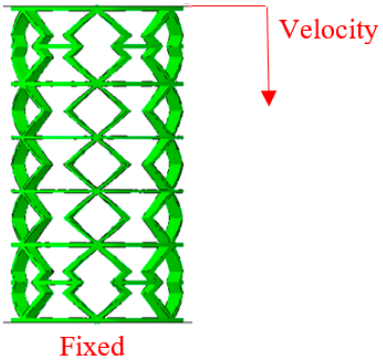

Figure 8. Boundary conditions in the FEA.

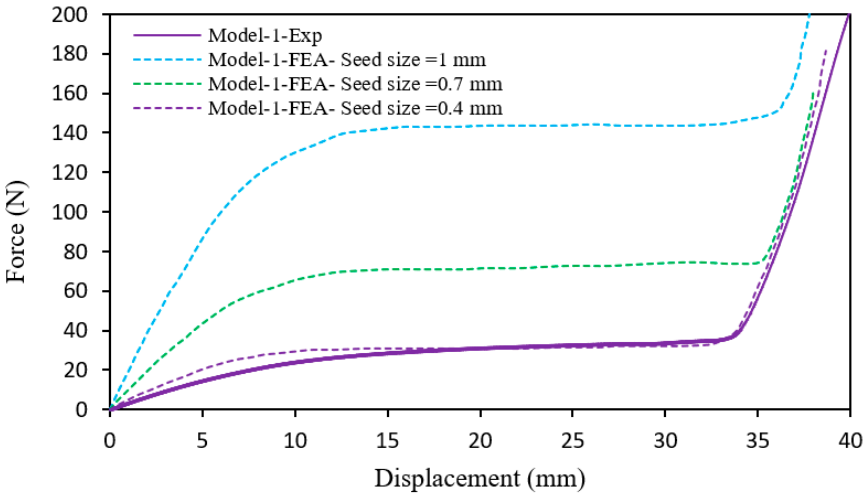

Figure 9. Mesh convergence study.

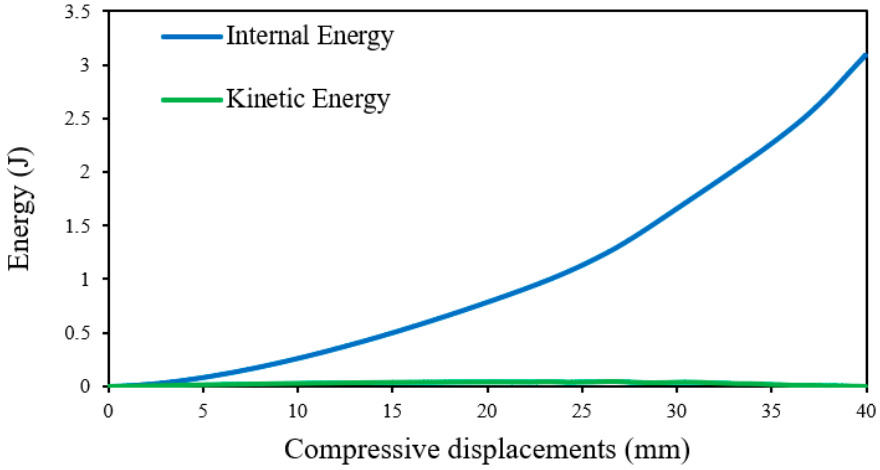

Figure 10. A comparison between internal and kinetic energy obtained from the FEA related to model 1.

3. Results and Discussions

3.1. A Comparison between Soft and Stiff Re-Entrant Unit Cells

To have a deeper understanding of "soft and stiff" re-entrant unit cells and why they are named so, two cylindrical tubes with the same repetitions of the unit cells (five times and four times, axial and radial repetitions, respectively) were considered, as illustrated in Figure 2. Figure 11 shows the deformation patterns of the cylindrical tubes under compression, possessing instabilities at high displacements. This is the main reason why the graded cylindrical metamaterials with the diversity in unit cell designs of "soft and stiff re-entrant unit cells" are introduced. In essence, the graded cylindrical metamaterials comprise soft and stiff cells to adjust the unit cell densifications (discussed in detail in the next sections). Finally, Figure 12 shows the higher stiffness of the stiff re-entrant unit cell compared with the soft re-entrant unit cells, as the curve slope in the elastic region related to the stiff cylinder is greater than that of the soft cylinder. Additionally, the soft cylinder possesses a softening behavior after 15 mm of displacement. On the contrary, apart from the instabilities at high compressive displacements, the stiff cylinder exhibits a hardening behavior. The displacement zone between 20 mm and 40 mm in Figure 12 indicates the overcoming of initial resistance of soft and stiff cylinders under compression.

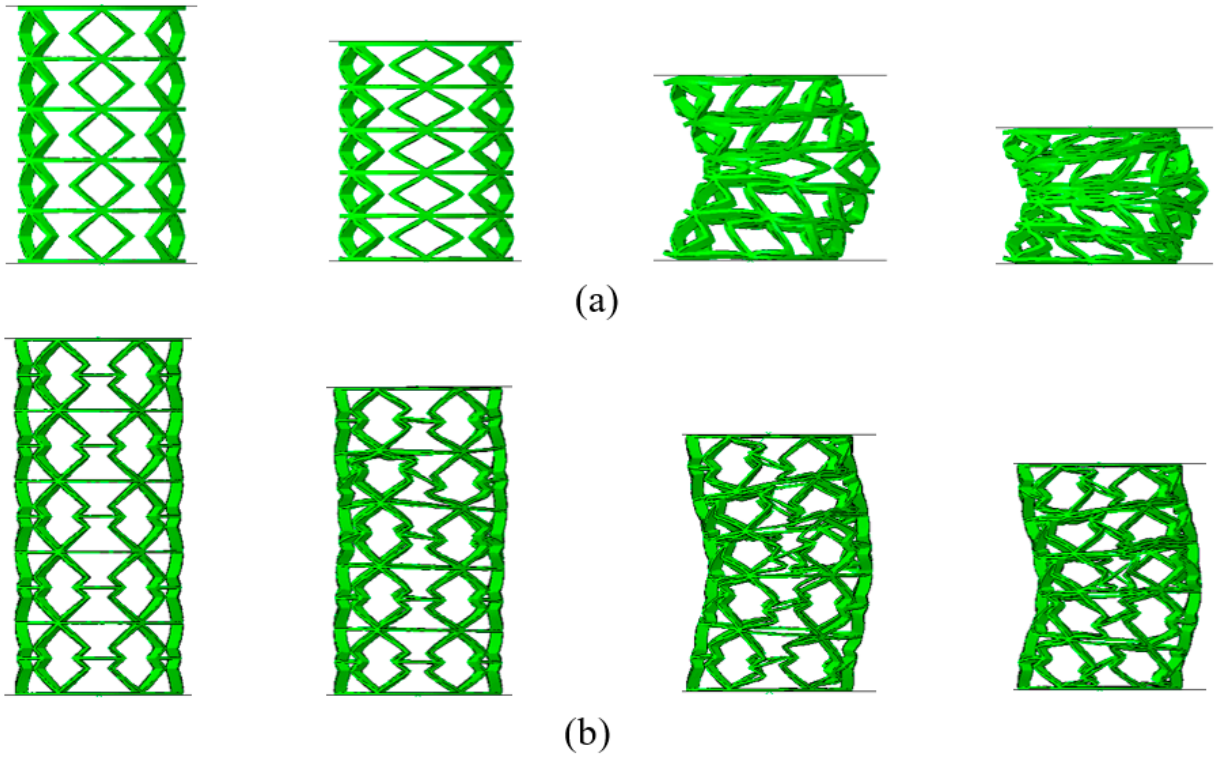

Figure 11. The deformation mechanisms of (**a**) soft and (**b**) stiff cylindrical tubes, shown in Figure 2, under compression.

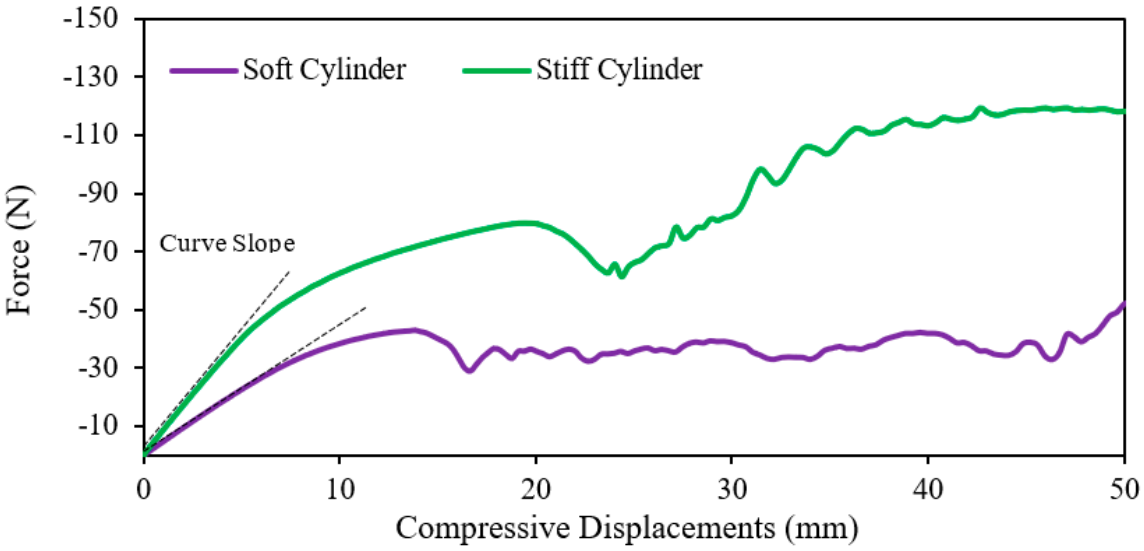

Figure 12. The force-displacement relation related to soft and stiff cylinders, shown in Figure 2, obtained from the FEA.

3.2. Deformation Patterns

This section describes the deformation patterns of ZPR cylindrical metamaterials containing the simultaneous "soft" and "stiff" unit cells. As can be seen in Figure 13, when the compressive displacements are applied, the "stiff" unit cells lead to the densification of "soft" unit cells first. This is the considerable variability in the stiffness of the unit cells that gives rise to the occurrence of a plateau region (zero stiffness) in the force-displacement relationship. By analyzing the compressive behavior of the metamaterials, the force-displacement relations can be divided into three main parts (see Figure 14). The positive stiffness region (region I) is due to the compression of "soft" unit cells until overcoming the soft unit cells' initial resistance. In fact, this region acts as a linear spring with positive stiffness. Then, the QZS region (region II) is caused by the densification of the soft unit cells, but not the collapse of stiff unit cells (see the region shown in the red rectangle in Figure 13). Finally, region III is where the full densification of cylinders under compression begins, resulting in an upward trend in the force-displacement relationship. Comparing the deformation patterns between FEA results and experiments, they exhibit good agreements in terms of deformation patterns under compression (see Figure 13).

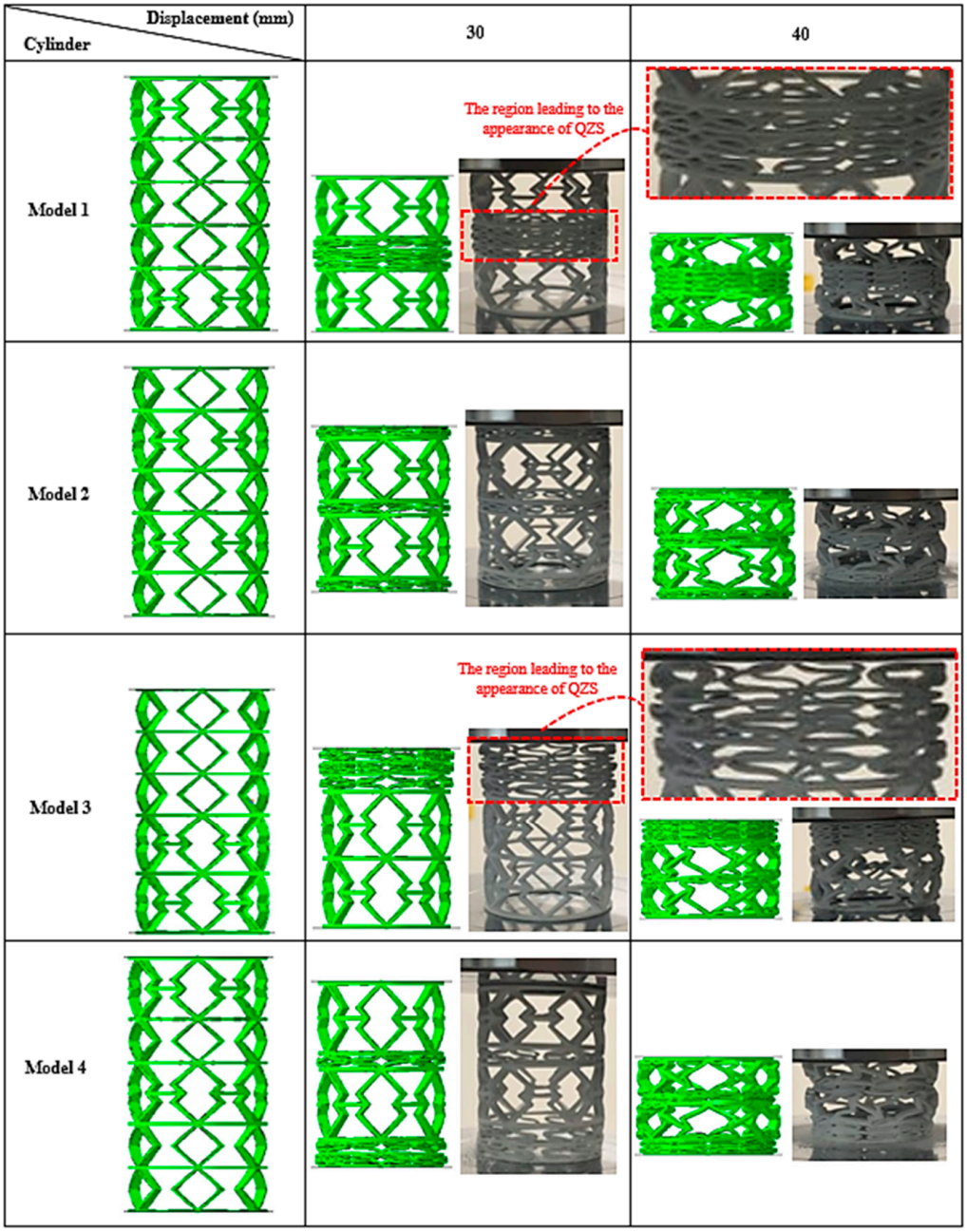

Figure 13. The comparison of deformation mechanisms between experiments and the FEA of cylinders Models 1–4.

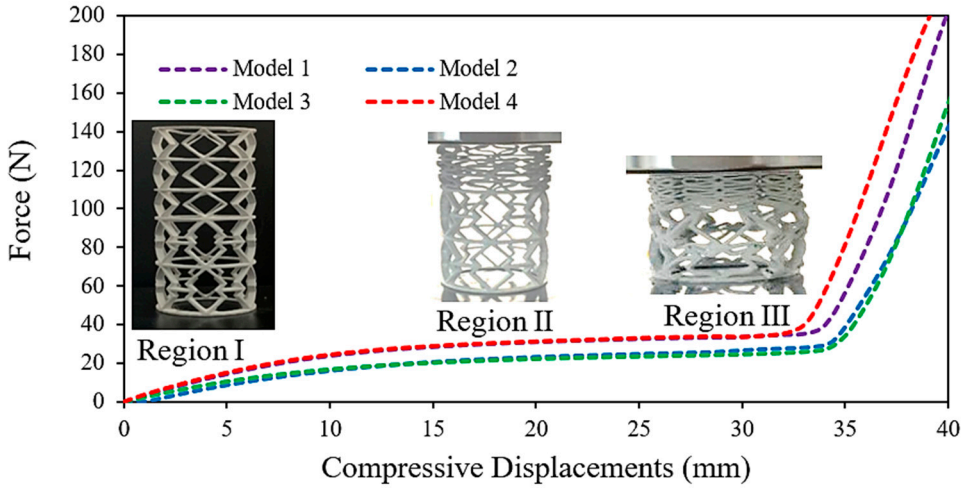

Figure 14. The force-displacement relations of the cylinders under compression obtained from the experiments.

3.3. Control of Global Buckling

Cylindrical structures are widely considered for various industries, ranging from automobile to aerospace industries [30,31]. What makes the cylindrical structures superior to the lattice panels is their capability to carry high levels of axial and/or transverse compressive loadings [32]. From a mechanical standpoint, cylindrical structures mainly experience two types of buckling under axial compression: local and global buckling [33,34]. In local buckling, though the axis of the cylindrical structures remains straight and unchanged, the cylindrical structure's cross-section buckles, leading to the formation of different sectional areas. Whereas, when it comes to global buckling, the axis of the cylindrical tube faces abrupt changes in its position. As mentioned earlier, the specific arrangement of soft and stiff re-entrant unit cells leads to controlling the global buckling of the cylindrical tubes under compression (see Section 3.2). However, the perennial question that comes to mind is what would happen if a long cylindrical tube compresses. In this situation, even though the specific arrangement of "soft and stiff re-entrant unit cells" plays a crucial role in controlling global buckling, the role of multi-thickness unit cells is hard to ignore. Indeed, graded metamaterials can be created by varying cell wall thickness, unit cell configurations, or both. As depicted in Figure 15, a cylindrical tube with a high length to diameter ratio of (L/D = 3.7) and constant cell wall thicknesses possesses global buckling under compression. On the contrary, the same cylindrical tube with multi-thickness unit cells possesses the capability of controlling global buckling. This means that using different unit cells' configurations and multi-thickness walls leads to adjusting the cylindrical tube's local stiffness, resulting in controlling the unit cells' collapse and densification. Consequently, the proposed soft and stiff unit cell configurations with simultaneous multi-thickness walls can densify the cylindrical metamaterial layer-by-layer to avoid the occurrence of global buckling. Figure 15b shows the hierarchy of unit cells' densifications under compression.

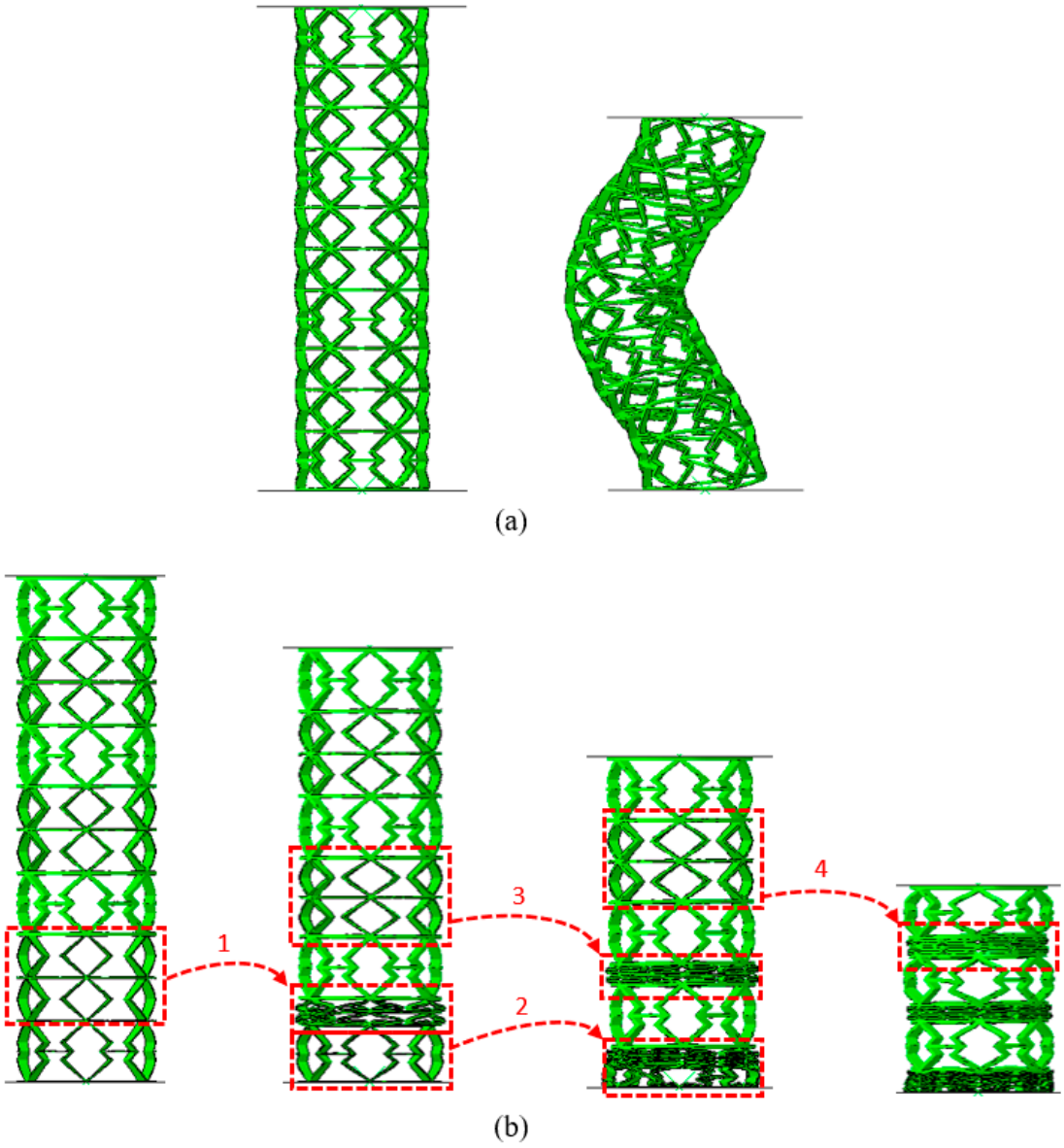

Figure 15. The deformation patterns of long cylinders with (**a**) the same and (**b**) multi-thickness cell walls, shown in Figure 2, under compression.

3.4. Vibration Isolation Capability

To provide stability for the whole model under external excitation, as each cylindrical metamaterial exhibits QZS (see Section 3.2), it is more logical to take all cylindrical metamaterials into account during experiments instead of evaluating the vibration performance of each cylindrical metamaterial separately (see Figure 16).

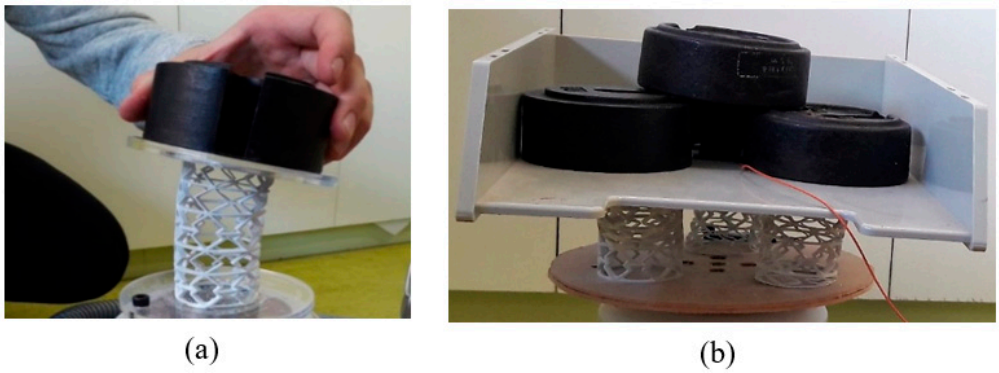

Figure 16. The (**a**) instability of one and (**b**) the stability of four cylindrical metamaterials under vibration test.

As discussed previously (see Section 3.2), the force-displacement relationship of the cylindrical metamaterials contains three main parts, including two positive stiffness regions (regions I and III) and one quasi-zero region (region II). When an object is placed on the cylindrical metamaterials, its weight is mainly supported by the positive stiffness region I. When an equilibrium condition is established, the QZS appears in the force-displacement relationship. In fact, the object will be isolated based on the QZS region II (the plateau region in the force-displacement relationship). Afterward, sinusoidal excitations are applied to the bottom plate via the shaker. Figure 17 shows the soft unit cells' compression leading to vibration isolation in cylindrical metamaterials. Figure 18 demonstrates the evaluation of the 3D-printed graded cylindrical metamaterials under different vibration scenarios, including an average amplitude of 0.03 G (0.29 m/s^2), 0.064 G (0.63 m/s^2), 0.09 G (0.88 m/s^2), and 0.11 G (1.1 m/s^2). As shown in Figure 18, the proposed cylindrical metamaterials exhibit the capability of isolating external excitations at low frequencies, ranging from 10 to 30 Hz, mainly before the resonance peaks. This is the most remarkable characteristic of the cylindrical metamaterials designed in this study. In other words, the more negative the VLD parameter becomes, the better vibration isolation performance the cylindrical metamaterials possess. This characteristic conflicts with linear isolators experiencing large static deflection to obtain a low natural frequency. Evidence of vibration isolation before resonant peaks is a phenomenon that is quite challenging to achieve with traditional vibration isolators.

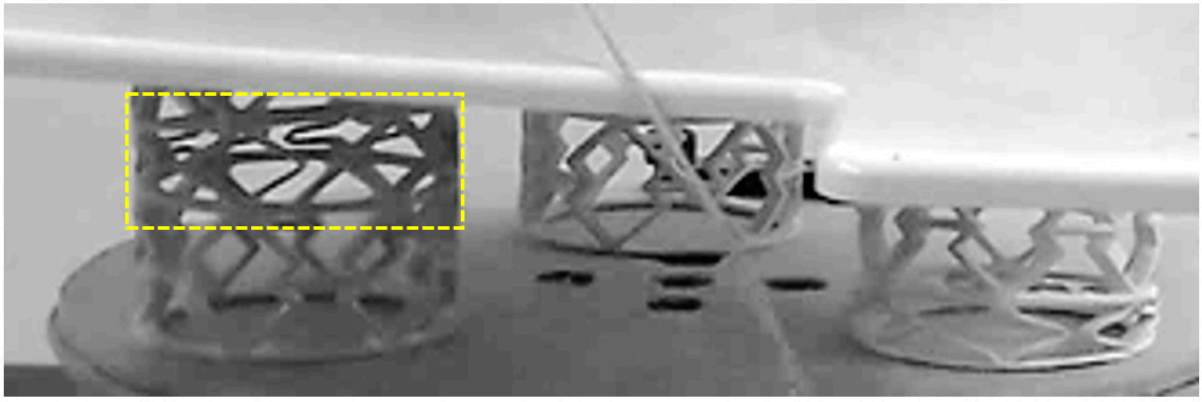

Figure 17. The compression of soft unit cells under external excitations.

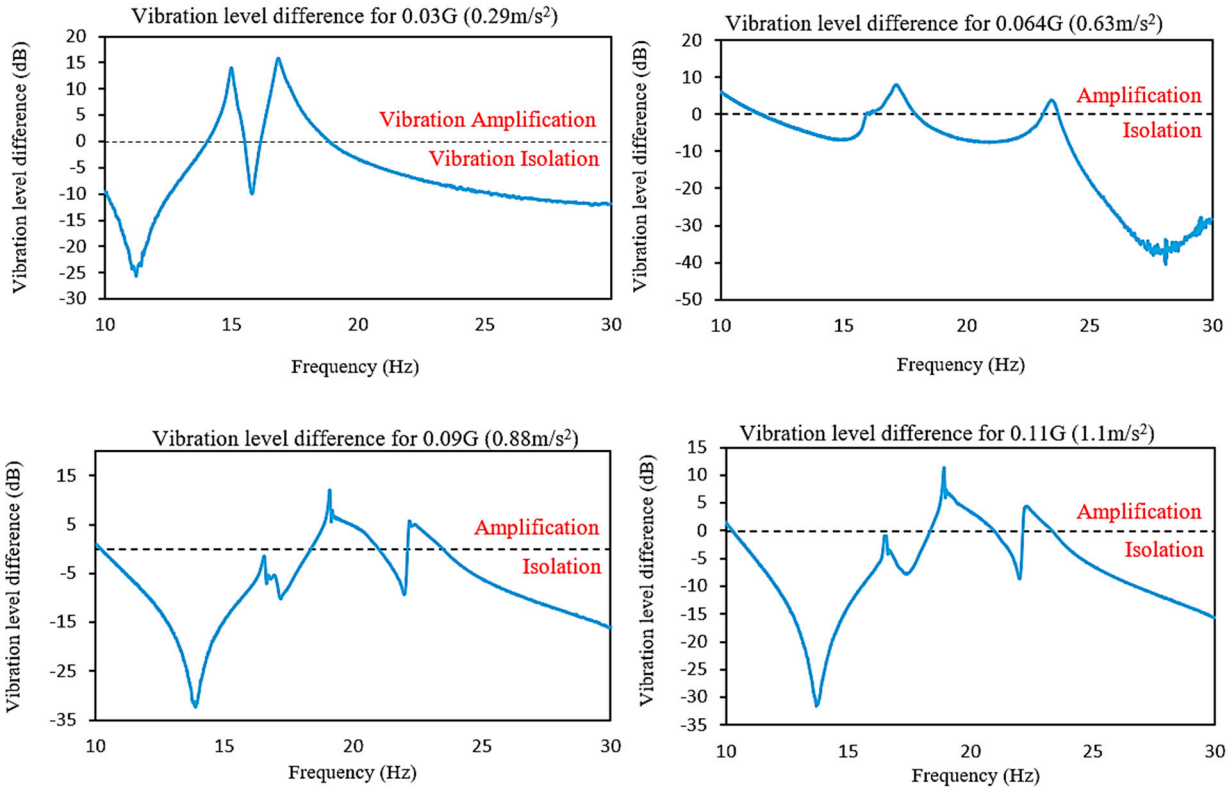

Figure 18. VLD for different input accelerations related to the comfort level of human body obtained from vibration tests on the Models (1–4).

4. Concluding Remarks

This study introduced novel 3D-printed graded cylindrical metamaterials for fulfilling two main aims: isolating external excitations in low-frequency ranges before vibration resonance and controlling long cylinders' global buckling under compression. The findings are summarized as follows:

- "Soft and stiff" re-entrant unit cells with varying stiffness are introduced.
- The different unit cells' configurations and cell-wall thicknesses are considered the gradient items.
- The variability in the unit cells' stiffness is caused by the specific designs of the unit cells, as shown by simulation using the finite element method and verified using experimental results.
- The variability in the unit cells' stiffness leads to controlling the unit cells' densification throughout the cylindrical metamaterial under compression. This means that the cylindrical metamaterials comprise a specific arrangement of the unit cells, leading to controlling long cylindrical tubes' global buckling (cylindrical tubes with a 3.7 length to diameter ratio).
- The considerable difference in "soft and stiff" unit cells' stiffness leads to the appearance of quasi-zero stiffness (QZS) in the force-displacement relationship under compression, making the graded cylindrical metamaterials superior in terms of vibration isolation over the conventional isolators.
- Unlike conventional springs, graded cylindrical metamaterials can isolate selective external excitations in low-frequency ranges from 10 to 30 Hz, verified through experimental vibration tests. These frequency ranges are related to the subjective comfort levels experienced by the human body in off-road vehicles.

Author Contributions: Conceptualization, A.Z., M.B. and R.H.; Formal analysis, M.F. and B.F.R.; Funding acquisition, A.Z. and B.F.R.; Investigation, A.Z., R.H., M.B. and L.P.; Methodology, A.Z., M.B., R.H. and L.P.; Project administration, A.Z., M.F. and B.F.R.; Supervision, A.Z., M.B. and B.F.R.; Validation, L.P. and R.H.; Writing—original draft, A.Z., M.B., L.P. and R.H.; Writing—review & editing, all authors equally contributed in reviewing this manuscript. All authors have read and agreed to the published version of the manuscript.

Funding: The authors would like to thank Department of Industry, Science, Energy and Resources project AEGP000029, the School of Engineering, and the Faculty of Science, Engineering, and Built Environment, Deakin University for their financial support.

Data Availability Statement: The data that support the findings of this study are available from the corresponding author, A.Z., upon reasonable request.

Conflicts of Interest: The authors declare no conflict of interest.

References

1. Zhang, W.; Zhang, B.; Fang, X.; Cheng, K.; Chen, W.; Wang, Z.; Hong, D.; Zhang, M. Microfluid-based soft metasurface for tunable optical activity in THz wave. *Opt. Express* **2021**, *29*, 8786–8795. [CrossRef] [PubMed]
2. Zhang, W.; Zhang, M.; Yan, Z.; Zhao, X.; Cheng, J.; Liu, A.Q. Single mode to dual mode switch through a THz reconfigurable metamaterial. *Appl. Phys. Lett.* **2017**, *111*, 241106. [CrossRef]
3. Moeini, M.; Begon, M.; Lévesque, M. Numerical homogenization of a linearly elastic honeycomb lattice structure and comparison with analytical and experimental results. *Mech. Mater.* **2022**, *167*, 104210. [CrossRef]
4. Abdulaziz, A.H.; Hedaya, M.; Elsabbagh, A.; Holford, K.; McCrory, J. Acoustic emission wave propagation in honeycomb sandwich panel structures. *Compos. Struct.* **2021**, *277*, 114580. [CrossRef]
5. Wei, Y.; Zhang, Y.; Song, Q.; Zhou, X.; Zhou, Y.; Shen, Y. Effects of different configurations and gradients on compression responses of gradient honeycombs via selective laser melting. *Thin-Walled Struct.* **2022**, *170*, 108462. [CrossRef]
6. Dong, J.; Fan, H. Crushing behaviors of buckling-oriented hexagonal lattice structures. *Mech. Mater.* **2022**, *165*, 104160. [CrossRef]
7. Hamzehei, R.; Zolfagharian, A.; Dariushi, S.; Bodaghi, M. 3D-Printed Bio-inspired Zero Poisson's Ratio Graded Metamaterials with High Energy Absorption Performance. *Smart Mater. Struct.* **2022**, *31*, 035001. [CrossRef]
8. Hexiang, W.; Zhang, X.; Liu, Y. In-plane crushing behavior of density graded cross-circular honeycombs with zero Poisson's ratio. *Thin-Walled Struct.* **2020**, *151*, 106767.
9. Jha, A.; Dayyani, I. Shape optimisation and buckling analysis of large strain zero Poisson's ratio fish-cells metamaterial for morphing structures. *Compos. Struct.* **2021**, *268*, 113995. [CrossRef]
10. Hamzehei, R.; Rezaei, S.; Kadkhodapour, J.; Anaraki, A.P.; Mahmoudi, A. 2D triangular anti-trichiral structures and auxetic stents with symmetric shrinkage behavior and high energy absorption. *Mech. Mater.* **2020**, *142*, 103291. [CrossRef]
11. Rezaei, S.; Kadkhodapour, J.; Hamzehei, R.; Taherkhani, B.; Anaraki, A.P.; Dariushi, S. Design and modeling of the 2D auxetic metamaterials with hyperelastic properties using topology optimization approach. *Photon-Nanostructures Fundam. Appl.* **2021**, *43*, 100868. [CrossRef]
12. Mansoori, H.; Hamzehei, R.; Dariushi, S. Crashworthiness analysis of cylindrical tubes with coupling effects under quasi-static axial loading: An experimental and numerical study. *Proc. Inst. Mech. Eng. Part L J. Mater. Des. Appl.* **2022**, *236*, 647–662. [CrossRef]
13. Hamzehei, R.; Kadkhodapour, J.; Anaraki, A.P.; Rezaei, S.; Dariushi, S.; Rezadoust, A.M. Octagonal auxetic metamaterials with hyperelastic properties for large compressive deformation. *Int. J. Mech. Sci.* **2018**, *145*, 96–105. [CrossRef]
14. Iwai, A.; Righetti, F.; Wang, B.; Sakai, O.; Cappelli, M.A. A tunable double negative device consisting of a plasma array and a negative-permeability metamaterial. *Phys. Plasmas* **2020**, *27*, 023511. [CrossRef]
15. Elmadih, W.; Chronopoulos, D.; Zhu, J. Metamaterials for simultaneous acoustic and elastic bandgaps. *Sci. Rep.* **2021**, *11*, 14635. [CrossRef] [PubMed]
16. Zhang, Q.; Guo, D.; Hu, G. Tailored Mechanical Metamaterials with Programmable Quasi-Zero-Stiffness Features for Full-Band Vibration Isolation. *Adv. Funct. Mater.* **2021**, *31*, 2101428. [CrossRef]
17. Zhakatayev, A.; Kappassov, Z.; Varol, H.A. Analytical modeling and design of negative stiffness honeycombs. *Smart Mater. Struct.* **2020**, *29*, 045024. [CrossRef]
18. Noroozi, R.; Bodaghi, M.; Jafari, H.; Zolfagharian, A.; Fotouhi, M. Shape-Adaptive Metastructures with Variable Bandgap Regions by 4D Printing. *Polymers* **2020**, *12*, 519. [CrossRef]
19. Wang, K.; Zhou, J.; Ouyang, H.; Cheng, L.; Xu, D. A semi-active metamaterial beam with electromagnetic quasi-zero-stiffness resonators for ultralow-frequency band gap tuning. *Int. J. Mech. Sci.* **2020**, *176*, 105548. [CrossRef]
20. Wang, L.; Zhao, Y.; Sang, T.; Zhou, H.; Wang, P.; Zhao, C. Ultra-low frequency vibration control of urban rail transit: The general quasi-zero-stiffness vibration isolator. *Veh. Syst. Dyn.* **2021**, *60*, 1788–1805. [CrossRef]
21. Suman, S.; Balaji, P.S.; Selvakumar, K.; Kumaraswamidhas, L.A. Nonlinear Vibration Control Device for a Vehicle Suspension Using Negative Stiffness Mechanism. *J. Vib. Eng. Technol.* **2021**, *9*, 957–966. [CrossRef]

22. Zolfagharian, A.; Denk, M.; Bodaghi, M.; Kouzani, A.Z.; Kaynak, A. Topology-Optimized 4D Printing of a Soft Actuator. *Acta Mech. Solida Sin.* **2019**, *33*, 418–430. [CrossRef]
23. Guo, L.; Wang, X.; Fan, R.-L.; Bi, F. Review on Development of High-Static–Low-Dynamic-Stiffness Seat Cushion Mattress for Vibration Control of Seating Suspension System. *Appl. Sci.* **2020**, *10*, 2887. [CrossRef]
24. Fan, H.; Yang, L.; Tian, Y.; Wang, Z. Design of metastructures with quasi-zero dynamic stiffness for vibration isolation. *Compos. Struct.* **2020**, *243*, 112244. [CrossRef]
25. Zhao, F.; Ji, J.; Luo, Q.; Cao, S.; Chen, L.; Du, W. An improved quasi-zero stiffness isolator with two pairs of oblique springs to increase isolation frequency band. *Nonlinear Dyn.* **2021**, *104*, 349–365. [CrossRef]
26. Cai, C.; Zhou, J.; Wu, L.; Wang, K.; Xu, D.; Ouyang, H. Design and numerical validation of quasi-zero-stiffness metamaterials for very low-frequency band gaps. *Compos. Struct.* **2020**, *236*, 111862. [CrossRef]
27. Xu, L.; Chai, X.; Gao, Z.; Li, Y.; Wang, Y. Experimental study on driver seat vibration characteristics of crawler-type combine harvester. *Int. J. Agric. Biol. Eng.* **2019**, *12*, 90–97. [CrossRef]
28. Abaqus. 2019ABAQUS User's Manual. Version 6.14. Available online: http://130.149.89.49:2080/v6.14/books/usb/default.htm (accessed on 30 May 2022).
29. Dai, M.; Jiang, H.; Dai, X.; Chen, G.; Yang, F.; He, X. Investigations of the compressive mechanical properties of open-cell hollow-sphere structures. *Mech. Mater.* **2020**, *148*, 103517. [CrossRef]
30. Araújo, H.; Leite, M.; Ribeiro, A. The effect of geometry on the flexural properties of cellular core structures. *Proc. Inst. Mech. Eng. Part L J. Mater. Des. Appl.* **2019**, *233*, 338–347. [CrossRef]
31. Hussain, N.N.; Regalla, S.P.; Rao, Y.V.D.; Dirgantara, T.; Gunawan, L.; Jusuf, A. Drop-weight impact testing for the study of energy absorption in automobile crash boxes made of composite material. *Proc. Inst. Mech. Eng. Part L J. Mater. Des. Appl.* **2021**, *235*, 114–130. [CrossRef]
32. Bodaghi, M. Reversible energy absorbing meta-sandwiches by FDM 4D printing. *Int. J. Mech. Sci.* **2020**, *173*, 105451. [CrossRef]
33. Xu, X.; Ma, J.; Lim, C.; Chu, H. Dynamic local and global buckling of cylindrical shells under axial impact. *Eng. Struct.* **2009**, *31*, 1132–1140. [CrossRef]
34. Noroozi, R.; Shamekhi, M.A.; Zolfagharian, A.; Asgari, F.; Mousavizadeh, A.; Bodaghi, M.; Haghighipour, N. In vitro static and dynamic cell culture study of novel bone scaffolds based on 3D-printed PLA and cell-laden alginate hydrogel. *Biomed. Mater.* **2022**. [CrossRef] [PubMed]